P Selected for a Viewpoint in *Physics*

PHYSICAL REVIEW LETTERS

℘

Visualizing Electronic Chirality and Berry Phases in Graphene Systems Using Photoemission with Circularly Polarized Light

Y. Liu,[1,2] G. Bian,[1,2] T. Miller,[1,2] and T.-C. Chiang[1,2]

[1]*Department of Physics, University of Illinois at Urbana-Champaign, 1110 West Green Street, Urbana, Illinois 61801-3080, USA*
[2]*Frederick Seitz Materials Research Laboratory, University of Illinois at Urbana-Champaign,*
104 South Goodwin Avenue, Urbana, Illinois 61801-2902, USA
(Received 23 July 2011; published 10 October 2011)

Electronic chirality near the Dirac point is a key property of graphene systems, which is revealed by the spectral intensity patterns as measured by angle-resolved photoemission spectroscopy under various polarization conditions. Specifically, the strongly modulated circular patterns for monolayer (bilayer) graphene rotate by $\pm 90°$ ($\pm 45°$) in changing from linearly to circularly polarized light; these angles are directly related to the phases of the wave functions and thus visually confirm the Berry's phase of π (2π) around the Dirac point. The details are verified by calculations.

Electronic chirality and the Berry's phase are topics of central importance to graphene physics [1–3]. The direction of the isospin vector in monolayer graphene tracks the rotation of the electronic crystal momentum, resulting in a Berry's phase of π [4,5]. By contrast, the isospin in bilayer graphene rotates twice as fast, resulting in a Berry's phase of 2π [6,7]. These unusual phase properties in graphene systems lead to an unconventional quantum Hall effect, which has attracted widespread interest in utilizing graphene as a new platform for electronic applications [1]. Angle-resolved photoemission spectroscopy (ARPES) has been employed extensively to examine the conical band dispersion relations [8,9]. Previous studies of monolayer graphene, using either s or p polarized light, show that the intensity patterns have a cosine functional form with a maximum along the ΓK direction [9–13]. Another study found that the intensity pattern for bilayer graphene from s polarized light has two nodes along the ΓK direction, which can be linked to the Berry's phase [14].

In this work, we employ ARPES with both circularly and linearly polarized light to probe the phase relations of the wave functions. While these relations are already known from simple tight-binding models, the use of circularly polarized light allows direct sensing of the phases in a visual manner. Specifically, the strongly modulated circular patterns for monolayer (bilayer) graphene rotate by $\pm 90°$ ($\pm 45°$) in changing from linearly to circularly polarized light. These angles and directions of rotation are determined by the phase angle of the incident light polarization, and arise from the interplay between electronic chirality and coherent interference of dipole transitions from the s and p polarization components. The observed ARPES patterns are in excellent agreement with calculations. The phases of electronic wave functions are hard to extract in general, but the information is critical for a number of systems including, apart from graphenes,

topological insulators, complex oxides, and magnetically ordered materials. Our work on graphene layers as model systems demonstrates that photoemission with circularly polarized light is a powerful approach to solve the phase problem.

Our ARPES measurements were performed at the Synchrotron Radiation Center, University of Wisconsin-Madison, using the new U9 VLS-PGM beam line. All spectra were taken with the sample temperature at 60 K. The polarization purity is better than 99% for HP and VP, and better than 80% for LCP and RCP. The accuracy of sample alignment with respect to light polarization is better than 2°. Monolayer and bilayer graphene samples were prepared on the Si-face of a 6H SiC (0001) substrate by graphitization of the surface in an atmosphere of 10^{-6} Torr of disilane to ensure growth of graphene layers with large domain sizes [15,16]. The coverage of graphene layers, excluding the $6\sqrt{3} \times 6\sqrt{3}$ buffer layer, is deduced from the Dirac-cone feature near the K point [17–19].

Our ARPES geometry and the coordinate system in relation to the graphene atomic structure and the Brillouin zone are shown in Figs. 1(a)–1(c). Four polarization configurations were employed: horizontal polarization (HP, or p polarization), vertical polarization (VP, or s polarization), left circular polarization (LCP) and right circular polarization (RCP). The geometry is such that the vector potential **A** of the incident light lies nearly within the sample plane; thus A_z can be ignored to first order. Figure 1(d) shows ARPES results around the K point measured along the y direction with LCP and RCP. Evidently, photons with different helicity selectively excite one of the two branches of the Dirac cone with opposite isospin directions. The observed difference can be characterized by a dichroism coefficient, D, defined as

$$D = \pm(I_4 - I_3)/(I_1 + I_2), \qquad (1)$$

(a)

(b)

(c)

(d)

(a)

(b)
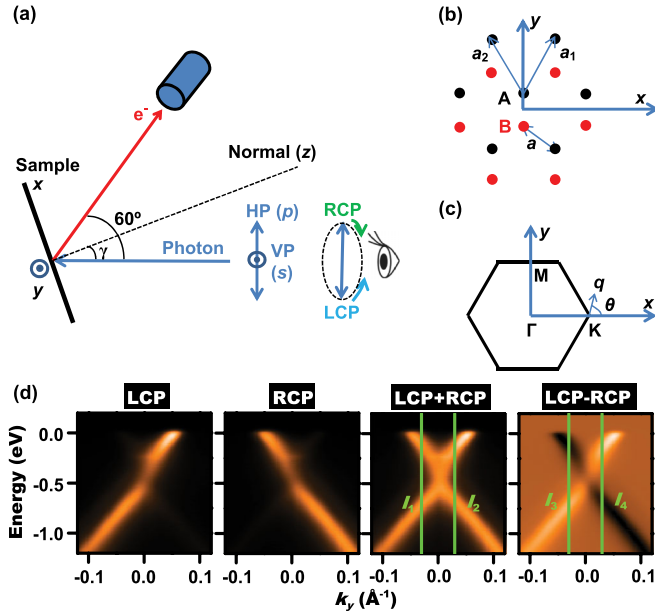
FIG. 1 (color online). Experimental geometry and circular dichroic data. (a) Schematic of experimental setup. HP and VP correspond to p and s polarizations, respectively. Looking toward the sample, LCP (RCP) corresponds to counterclockwise (clockwise) rotation of the electric field vector. (b) Coordinate system relative to the atomic structure of a monolayer graphene. (c) Surface Brillouin zone. **q** is wave vector measured from K. (d) Photoemission spectra from monolayer graphene near the K point measured along y using 30 eV photons. The four panels correspond to LCP, RCP, their sum and difference.

FIG. 2 (color online). ARPES data from monolayer graphene taken with HP, VP, LCP, and RCP using 30 eV photons. The Dirac point is at -0.45 eV. (a) Constant energy maps at -0.05 eV. (b) Constant energy maps at -0.9 eV. The right panels show the intensity of each semicircular arc as a function of θ. Each intensity curve has been normalized to unity maximum intensity.

where I_1, I_2, I_3, and I_4 are peak intensities of the energy distribution curves as specified in Fig. 1(d), and the $+$ and $-$ signs correspond to the π^* and π bands, respectively. Measurements show that D is close to unity near the K point at 30 eV photon energy. This large dichroic effect results from the different characters of the initial states on the two branches of the Dirac cone; the variations in the photoemission final states are negligible over the narrow range in reciprocal space [20].

Figures 2(a) and 2(b) show typical constant energy maps of the π^* and π bands of monolayer graphene, respectively, using the four polarization configurations. For each band, the semicircular pattern rotates counterclockwise in 90° steps in going from HP to LCP to VP and to RCP. Furthermore, the patterns of the π^* and π bands are related by inversion. The plots on the right-hand side of Fig. 2 show the measured intensity variations of the semicircular arc patterns about the azimuthal angle θ of the wave vector **k** relative to the K point [Fig. 1(c)]. The results are well described by cosine functional forms related by 90° offsets. These angular offsets are related to the phase of the initial state wave functions, $\Psi_i^{\mathbf{k}}$, which are given, to first order, by

$$\Psi_i^k(\mathbf{r}) \propto \sum_j \exp(i\mathbf{k} \cdot \mathbf{R}_j)\left[e^{i\theta/2}\phi\left(\mathbf{r} - \mathbf{R}_j - \frac{a}{2}\hat{y}\right)\right.$$
$$\left. \pm\, e^{-i\theta/2}\phi\left(\mathbf{r} - \mathbf{R}_j + \frac{a}{2}\hat{y}\right)\right], \quad (2)$$

where $\mathbf{R}_j$ is a lattice vector, ϕ is the carbon p_z orbital, a is the C-C bond length, and the summation is over all lattice vectors. The $+$ and $-$ signs correspond to the π^* and π bands, respectively. The phase factors associated with the two sublattices, $e^{\pm i\theta/2}$, determine the chiral properties of the electronic states and give rise to a Berry's phase of π upon incrementing the azimuthal angle θ by 2π.

The allowed final state of photoemission $\Psi_f^{\mathbf{k}}$ near the K point must be of even parity with respect to reflection about the xz plane. A straightforward calculation yields the photoemission intensities for the π^* and π bands [20]:

$$I \propto |A_x\xi_x(e^{i\theta/2} \pm e^{-i\theta/2}) + A_y\xi_y(e^{i\theta/2} \mp e^{-i\theta/2})|^2$$

$$= \begin{cases} 4\cos^2\frac{\theta}{2}|A_x|^2|\xi_x|^2 + 4\sin^2\frac{\theta}{2}|A_y|^2|\xi_y|^2 + 4\sin\theta\,\mathrm{Im}(A_x\xi_x A_y^*\xi_y^*), \\ 4\sin^2\frac{\theta}{2}|A_x|^2|\xi_x|^2 + 4\cos^2\frac{\theta}{2}|A_y|^2|\xi_y|^2 - 4\sin\theta\,\mathrm{Im}(A_x\xi_x A_y^*\xi_y^*) \end{cases} \quad (3)$$

where ξ_x and ξ_y are the dipole transition matrix elements for the carbon p_z orbital excited by the x and y components of the vector potential, A_x and A_y, respectively. With $A_y = 0$ for HP and $A_x = 0$ for VP, the first and second terms on the right-hand side of Eq. (3) yield the patterns excited by HP and VP, respectively. The results, proportional to $1 \pm \cos(\theta)$, are in good agreement with experiment [13]. However, the results are independent of the sign of θ. A transformation $\theta \rightarrow -\theta$ reverses the phases of the chiral electronic states [Eq. (2)], but leaves the intensity patterns invariant. Thus, measurements based on HP and VP alone are insufficient to fully determine the chiral phase relationships.

This indetermination can be resolved by using circularly or elliptically polarized light, for which the third term on the right-hand side of Eq. (3) comes into play. This term contains a factor of $\sin(\theta)$, an odd function of θ; thus, these measurements should uniquely specify the sense of θ. At 30 eV, $\xi_x \approx \xi_y$ as will be shown below. With A_x being real and A_y being imaginary for elliptical polarization, the photoemission intensity is reduced to

$$I \propto 2|\xi_x|^2 A_0^2[1 \pm \cos(\theta + 2\chi)], \quad (4)$$

where $A_0^2 = |A_x|^2 + |A_y|^2$ and $\chi = \arg(A_x + A_y)$ is the phase angle of the light polarization. Equation (4) shows that the intensity patterns have the same cosine forms as the case of linear polarization except for an angular offset of 2χ, or twice the phase angle of the elliptical polarization. A nonzero offset removes the sign ambiguity of θ; and the patterns become asymmetric with respect to the transformation $\theta \rightarrow -\theta$. With $\chi = -\pi/4, 0, \pi/4$ and $\pi/2$ for LCP, HP, RCP, and VP, respectively, the patterns should rotate clockwise in 90° steps following this sequence, which is indeed observed experimentally (Fig. 2). The third term in Eq. (3), resulting from interference between the dipole transitions excited by A_x and A_y, uniquely determines the direction of rotation.

The chirality of bilayer graphene is another interesting test case. The Dirac cone is split into two pieces. For the main cone at the Dirac point, the phase factors $e^{\pm i\theta/2}$ in Eq. (2) are replaced by $e^{\pm i\theta}$. Thus, the isospin rotates twice as fast as the monolayer case [7]. As a result, the intensity patterns become "compressed" by a factor of 2 as a function of θ. The single intensity maximum for the monolayer case for each polarization configuration becomes two intensity maxima separated by 180°. The angular offset for the different polarization configurations should become one half of the monolayer case, or 45°. Specifically, the two intensity maxima should be located at $\theta_{max} = \mp\chi$, $\mp\chi + \pi$, with the $-$ and $+$ signs corresponding to the

π^* and π bands, respectively. This is indeed seen in the experiment [Fig. 3(a)]. Because of the splitting of the Dirac cones, the photoemission intensity described by Eq. (4) should additionally be modified to include this effect [20]. This explains the other details of the data and why the intensity maximum at $\theta = \pi$ for HP appears missing [14,21]. Figure 3(b) shows the calculated intensity patterns, which agree well with the experiment. The characteristic 45° rotations of the intensity patterns between linear and circular polarizations, as well as the angular positions of the intensity maxima, are direct consequences
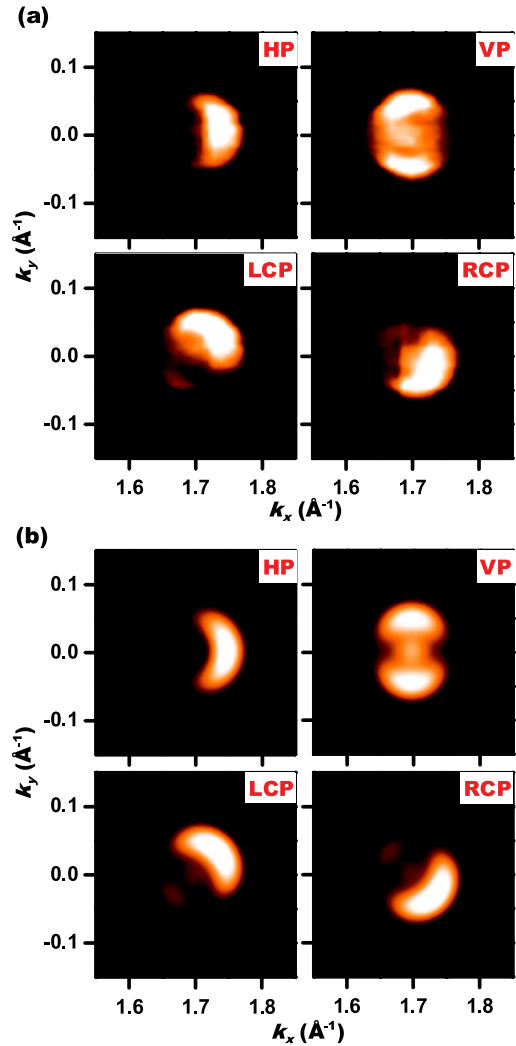
FIG. 3 (color online). ARPES data from bilayer graphene taken with HP, VP, LCP, and RCP using 30 eV photons. The Dirac point is at -0.3 eV. (a) Constant energy maps at -0.05 eV. (b) Calculated results with a Gaussian broadening of $\sigma = 0.015$ Å^{-1} in k space.

of the electronic chirality and a Berry's phase of 2π in bilayer graphene (vs. π in monolayer graphene).

The interference term in Eq. (3) depends on the phase difference between ξ_x and ξ_y. Let

$$\lambda e^{i\beta} = \xi_y / \xi_x, \qquad (5)$$

where λ and β are the amplitude ratio and phase difference, respectively, which can both depend on the photon energy because of variations in the final state. The amplitude ratio λ can be extracted from the intensity ratio ($= \lambda^2$) between VP and HP at $\theta = \pm\pi/2$ [Fig. 4(a)]. The phase difference β can be extracted from the measured dichroism coefficient D [Fig. 4(b)] via

$$\beta = \cos^{-1}\left(\frac{D(1 + \lambda^2)}{2\lambda}\right). \qquad (6)$$

The deduced β [Fig. 4(c)] is close to zero for photon energies above 30 eV, but increases at lower photon

FIG. 4 (color online). Deduction of the phase difference β for monolayer graphene. (a) The photoemission intensity ratio ($= \lambda^2$) between VP and HP at ±0.4 eV relative to the Dirac point as a function of photon energy. The "error bars" indicate the differences between results for the π^* and π bands. (b) The corresponding dichroism coefficient, D, obtained similarly. (c) The deduced phase difference (β) between transition matrix elements from HP and VP.

energies, where final-state band structure effects become significant [20,22]. Our results show that $\xi_x = \xi_y$ is well satisfied at 30 eV, which leads to very simple pattern rotations seen in Figs. 2 and 3. At high photon energies, band structure effects for the photoemission final states diminish, and we expect $\lambda \to 0$ and $\beta \to 0$ based on symmetry considerations [20]. However, an additional contribution from surface photoemission can come into play at very high photon energies [20,23–25], and the analysis can become more involved.

Our study thus shows that polarization-dependent ARPES can be a powerful tool for probing the phases of electronic wave functions in solids. While circular dichroic effects are well known in gas phase ARPES [26–28], much less has been studied for solid-state systems because of complications including electron correlation [29,30]. The Dirac Fermions in graphene systems are of special interest because of their chirality and nontrivial Berry's phases, which can be conveniently probed by elliptically polarized light with a built-in rotation of the vector field. Interference of the dipole transitions gives rise to the observed pattern rotations governed by the ellipticity of the incident light. This understanding and the methodology presented here should be useful for exploring other systems and problems including topological insulators, spin splittings and magnetic ordering. In particular, the surface states on topological insulators should have a nontrivial Berry's phase, and a recent photoemission study indeed revealed interesting circular dichroic effects [31,32]. Further analysis of the topological states based on the present method is underway.

[1] A. H. Castro Neto, F. Guinea, N. M. R. Peres, K. S. Novoselov, and A. K. Geim, Rev. Mod. Phys. **81**, 109 (2009).
[2] M. I. Katsnelson, K. S. Novoselov, and A. K. Geim, Nature Phys. **2**, 620 (2006).
[3] M. V. Berry, Proc. R. Soc. A **392**, 45 (1984).
[4] K. S. Novoselov et al., Nature (London) **438**, 197 (2005).
[5] Y. Zhang, Y.-W. Tan, H. L. Stormer, and P. Kim, Nature (London) **438**, 201 (2005).
[6] K. S. Novoselov et al., Nature Phys. **2**, 177 (2006).
[7] E. McCann and V. I. Fal'ko, Phys. Rev. Lett. **96**, 086805 (2006).

[8] S. Y. Zhou *et al.*, Nature Phys. **2**, 595 (2006).
[9] A. Bostwick, T. Ohta, T. Seyller, K. Horn, and E. Rotenberg, Nature Phys. **3**, 36 (2006).
[10] E. L. Shirley, L. J. Terminello, A. Santoni, and F. J. Himpsel, Phys. Rev. B **51**, 13 614 (1995).
[11] M. Mucha-Kruczyński *et al.*, Phys. Rev. B **77**, 195403 (2008).
[12] A. Bostwick *et al.*, Prog. Surf. Sci. **84**, 380 (2009).
[13] I. Gierz, J. Henk, H. Höchst, C. R. Ast, and K. Kern, Phys. Rev. B **83**, 121408(R) (2011).
[14] C. Hwang *et al.* Phys. Rev. B **84**, 125422 (2011).
[15] J. Hass, W. A. de Heer, and E. H. Conrad, J. Phys. Condens. Matter **20**, 323202 (2008).
[16] R. M. Tromp and J. B. Hannon, Phys. Rev. Lett. **102**, 106104 (2009).
[17] S. Y. Zhou *et al.*, Nature Mater. **6**, 770 (2007).
[18] T. Ohta *et al.*, Phys. Rev. Lett. **98**, 206802 (2007).
[19] Y. Liu *et al.*, Phys. Rev. Lett. **105**, 136804 (2010).
[20] See Supplemental Material at http://link.aps.org/supplemental/10.1103/PhysRevLett.107.166803 for additional data and details of the calculations.
[21] T. Ohta, A. Bostwick, T. Seyller, K. Horn, and E. Rotenberg, Science **313**, 951 (2006).
[22] H. Ohsawa *et al.*, Solid State Commun. **61**, 347 (1987).
[23] H. J. Levinson, E. W. Plummer, and P. J. Feibelman, Phys. Rev. Lett. **43**, 952 (1979).
[24] T. Miller, W. E. McMahon, and T.-C. Chiang, Phys. Rev. Lett. **77**, 1167 (1996).
[25] V. B. Zabolotnyy *et al.*, Phys. Rev. B **76**, 024502 (2007).
[26] S. Motoki *et al.*, Phys. Rev. Lett. **88**, 063003 (2002).
[27] T. Jahnke *et al.*, Phys. Rev. Lett. **88**, 073002 (2002).
[28] D. Dowek *et al.*, Phys. Rev. Lett. **104**, 233003 (2010).
[29] A. Kaminski *et al.*, Nature (London) **416**, 610 (2002).
[30] D. V. Vyalikh *et al.*, Phys. Rev. Lett. **100**, 056402 (2008).
[31] M. Z. Hasan, Physics **3**, 62 (2010).
[32] Y. H. Wang *et al.*, arXiv:1101.5636v1.